A&A 408, 1137–1154 (2003)
DOI: 10.1051/0004-6361:20030956

Astronomy & Astrophysics

Observations of the upper solar chromosphere with SUMER⋆

K. Wilhelm[1] and W. Kalkofen[2]

[1] Max-Planck-Institut für Aeronomie, Max-Planck-Str. 2, 37191 Katlenburg-Lindau, Germany
[2] Harvard-Smithsonian Center for Astrophysics, 60 Garden Street, Cambridge, MA 02138, USA
e-mail: wolf@cfa.harvard.edu

Received 11 March 2003 / Accepted 12 June 2003

Abstract. The structure and dynamics of the solar chromosphere are still matters of debate. The chromospheric network reflecting the supergranulation of the outer convection zone of the Sun is a prominent feature of the lower solar atmosphere that extends into the transition zone between chromosphere and corona. In particular, the physics of the so-called "nonmagnetic" chromosphere in internetwork regions as well as the physics of the magnetic network are not yet fully understood. Here we present observations of the H I Lyman continuum obtained in areas of the undisturbed Sun by the Solar Ultraviolet Measurements of Emitted Radiation (SUMER) instrument on the Solar and Heliospheric Observatory (SOHO). The observing sequences are unique in the sense that they cover the spectral range from 67 nm to 93 nm with the highest cadence the SUMER spectrometer can achieve operating near the limit of its mechanism performance, telemetry allocation, and memory capabilities. In this wavelength range not only the Lyman continuum but also many extreme-ultraviolet emission lines (N II, N III, S IV, O II, O III, O IV, O V, Ne VIII, and Mg IX) are prominent, allowing the investigation of radiation formed at temperatures representative of regions from the chromosphere to the corona. Brightenings have been identified that are presumed to be related to the well-known 3 min oscillations as seen, for instance, in Ca II H_{2v} and K_{2v} observations. The relative temporal variations of the continuum radiance near 77 nm were typically 20% to 40%, whereas simultaneously recorded transition-region lines varied by about 40% of their lowest values in phase with the continuum. In the corona, the Ne VIII and Mg IX lines with formation temperatures of 620 000 K and 950 000 K, respectively, experienced relative changes of ≈10% and displayed no phase relationship with the transition-region lines or the continuum. Radiance variations in the spatial regime across the solar disk show a higher correlation between the chromosphere and the corona than between the transition region and the corona. The observations will be discussed with a view towards providing constraints for modelling chromospheric structure and dynamics.

Key words. Sun: chromosphere – Sun: transition region – Sun: corona – Sun: UV radiation

1. Introduction

The discovery of the flash spectrum of a solar prominence, in particular the detection of the He I line D_3 at 587.5 nm by Janssen during the eclipse of 18 August 1868, and the identification of spicules by Secchi in 1877 mark the first detailed observations of chromospheric material. The chromospheric flash spectrum observed off the solar limb is characterized by emission lines that in many cases correspond to the Fraunhofer lines of the photosphere. The chromosphere can also be observed above the photosphere on the solar disk at various atmospheric densities with spectroheliographs by selecting narrow wavelength bands in strong Fraunhofer lines, such as Ca II H and K at 396.85 nm and 393.37 nm or Hα at 656.28 nm. These observations show a pronounced network structure in all areas of the undisturbed Sun (Deslandres 1899), which is related to velocity fields in the photosphere (Stuart & Rush 1954) and the supergranulation of the solar convection zone, with typical spatial scales of 30 Mm (Leighton et al. 1962). The network lanes contain magnetic-field concentrations, predicted by Parker (1963) and observed by Simon & Leighton (1964), with field strengths up to 0.2 T (2 kG) in the photosphere (Stenflo 1973), whereas only weak magnetic fields are present in internetwork regions (Livingston & Harvey 1971; Solanki 1993; De Pontieu 2002). Recently, small-scale fields of mixed polarity above 2 mT (20 G) have been measured in intergranular lanes (Domínguez Cerdeña et al. 2003).

Whether weak fields are important for the dynamics and the temperature structure of the internetwork medium is still an open question. A relationship of these weak fields in internetwork regions with Ca II grains was reported by Sivaraman & Livington (1982), but recent studies do not support a dependence of the grains on magnetic fields (Lites et al. 1999; Worden et al. 1999).

The grains have first been observed by Hale & Ellerman (1904) as "minute calcium flocculi". They are present on the

Send offprint requests to: K. Wilhelm,
e-mail: wilhelm@linmpi.mpg.de

⋆ Part of this work was carried out while KW was visiting the Harvard-Smithsonian Center for Astrophysics, Cambridge, MA, USA.

violet side of the Ca II H and K lines (Ca II H_{2v}, K_{2v}) as brightenings of the intermittent 3 min internetwork oscillations in the chromosphere, and are seen both in vertical motions and radiance[1] variations (Noyes & Leighton 1963; Orrall 1966; Noyes 1967; Liu 1974; Cram & Damé 1983; Rutten & Uitenbroek 1991). Steffens et al. (1996) found that only a fraction of 9% of the internetwork radiation field in K_{2v} is contributed by emission at the location of grains. Thus most of the emission comes from the dissipation of waves that heat the cell interior generally, and not from the large-amplitude waves that are responsible for the grains. The grains, therefore, have to be classified as relatively "rare" events. This may find support in a conclusion reached by Hoekzema et al. (2002) that extreme acoustic events in the photosphere are significantly correlated with excessive Ca II K_{2v} amplitudes.

Recent observations from the ground as well as from the Solar and Heliospheric Observatory (SOHO) of ESA and NASA, and the Transition Region and Coronal Explorer (TRACE) of NASA, with their combined high spatial, spectral and temporal resolution capabilities, made detailed investigations of the structure and dynamics of the chromosphere possible in many wavelength bands (e.g., Uitenbroek et al. 1994; Hofmann et al. 1996; Solanki et al. 1996; Steffens et al. 1997a,b; Hansteen 1997; Carlsson et al. 1997; Judge et al. 1997; Heinzel & Curdt 1998; Curdt et al. 1999; Doyle et al. 1999; Gouttebroze et al. 1999; Hansteen et al. 2000; Wikstøl et al. 2000; Muglach et al. 2000; Judge et al. 2001; Krijger et al. 2001; McIntosh et al. 2001). The observations confirmed earlier Ca II results (Lites et al. 1993) that internetwork and network regions show distinctly different temporal variations with typical oscillations near 3 min in the internetwork and longer periods in network lanes; the latter are not directly correlated with variations in the photosphere. No conclusive evidence of periods much shorter than 3 min could be found in internetwork areas. Oscillations of 3 min and 5 min periods both in radiance and line-of-sight velocity were also seen in VUV spectral lines by OSO-7 and OSO-8 instruments (Chapman et al. 1972; Chipman et al. 1976).

The spatial coherence lengths increase with the brightness or formation temperatures, T_B or T_F, of the lines or the continua[2], from a few seconds of arc in the Si I and C I continua ($T_B \approx 4500$ K) ($1'' \approx 4.85 \times 10^{-6}$ rad corresponds to approximately 700 km at the Sun; cf., Table 1) to 20″ and more in C III lines ($T_F \approx 80\,000$ K). For grains alone, on the other hand, the horizontal size of the bright regions tends to be much smaller, varying from less than 1″ for the 160 nm continuum (Foing & Bonnet 1984) to 5″ to 8″ for lines observed with the Solar Ultraviolet Measurements of Emitted Radiation (SUMER) instrument on SOHO (Carlsson et al. 1997). Radiance variations can easily be seen in spectral lines with low formation temperatures (i.e., emitted by neutrals or singly-charged ions), however, for third or higher spectra, only line-of-sight velocity oscillations with amplitudes of up to 10 km s^{-1} are prominent in internetwork regions. These regions are rather dark, yet, in all cases, emit radiation well above the background level of modern vacuum-ultraviolet (VUV) detectors. Using data from the High Resolution Telescope and Spectrograph (HRTS), Athay & Dere (1990) have specifically established that C I and O I lines show appreciable emission there, without gaps, on spatial-resolution scales slightly less than 1″.

The 3 min oscillations are sometimes viewed as the high-frequency portion of the sub-photospheric *p*-mode oscillations, which have a broad maximum near 5 min (Leighton et al. 1962; Schatzman & Souffrin 1967; Ulrich 1970; Deubner 1975; Cram 1978; Hofmann et al. 1996; Judge et al. 2001). But the location memory of the grains over many oscillation cycles, as seen, for example, in the observations of Damé (1984) and Lites et al. (1993) and modelled by Carlsson & Stein (1994), argues against this interpretation. As shown by Carlsson & Stein (1994, 1995, 1997), the 3 min oscillations in grains are due to propagating acoustic waves above the acoustic cutoff or critical frequency (Lamb 1908) in the solar atmosphere, whereas the 5 min oscillations are due to evanescent acoustic waves (cf., Balmforth & Gough 1990; Kumar 1993).

Based on 1932 eclipse observations of He I lines between 400.9 nm and 587.6 nm, Goldberg (1939) had determined a temperature of 4300 K at 670 km altitude above the limb and 6700 K at 2330 km, with uncertainties of several hundred kelvin. Biermann (1948) and Schwarzschild (1948) independently explained this temperature increase by outward-travelling sound waves that dissipate as shocks. Note, however, that Biermann's assumption of a so-called "UV excess", which was derived from ionospheric observations, was several orders of magnitude too high.

In all chromospheric observations, the spectral lines in the VUV range are seen in emission at all times and everywhere, both in internetwork regions and in network lanes. These findings imply a mean temperature increase of the chromosphere with height, as described in many chromospheric models, e.g., in VAL81 (Vernazza et al. 1981). The temperature model of Carlsson & Stein (1994), if valid to the upper chromosphere, would however predict absorption lines for most of the time throughout the internetwork chromosphere. Carlsson & Stein (1995) suggest a magnetic-field effect at higher altitudes, which leads to Mg II h and k lines in emission over the whole solar disk as observed by Lemaire & Skumanich (1973); but for radiation from the low and middle chromosphere, absorption lines are still predicted most of the time, contrary to observations.

The conclusion that the temperature increases with height above the temperature minimum everywhere was also reached by Zirin & Popp (1989), based on observations of the Mg I 12.3 μm line, which was seen in emission and with limb brightening. However, their assumption of a local thermodynamic-equilibrium (LTE) source function is not supported by numerical non-LTE models (Lemke & Holweger 1987; Hoang-Binh 1991; Chang et al. 1991; Carlsson et al. 1992), which place the formation height of the Mg I 12.3 μm emission in the upper photosphere, just below or at the temperature minimum of the solar atmosphere. Observations during the total eclipse of 11 July 1991 with a spatial resolution of 220 km showed indeed the maximum of the 12.3 μm line signal at ≈500 km above the

[1] For the use of "radiance" in line with the International System of Units see, e.g., Smith & Huber (2002) and Wilhelm (2002).

[2] For a definition of T_B see Sect. 3.2; T_F is the temperature of the maximum of the contribution function (Pottasch 1963).

limb in the visible continuum, but, in addition, significant line emission was detected to heights of more than 2 Mm (Deming et al. 1992). These authors suggest that spatial inhomogeneities contribute to this extension. It is thus questionable whether the infrared Mg I observations can be used as an argument for a standard chromospheric temperature structure.

Observations of the 4.7 μm carbon monoxide bands (Ayres 1981; Solanki et al. 1994; Ayres & Rabin 1996; Uitenbroek 2000) also appear to cast doubt on the standard chromospheric structure, because relatively cool gas (<4000 K) is thought to be present above the canonical temperature minimum at the photosphere-chromosphere interface, where the brightness temperature is 4500 K (Brekke & Kjeldseth-Moe 1994a)[3]. However, the analysis of HRTS data by Athay & Dere (1990) does not allow cool gas above the height of the temperature minimum, except in pockets with a size below 1″, which would not be thermally isolated. Thus the formation of CO emission lines off the solar limb remains to be explained. Brightness temperature oscillations of about ±100 K in CO lines with periods near 3 min have been reported by Uitenbroek et al. (1994), whereas predominantly 5 min oscillations were seen in velocities.

Recent simulations of large-amplitude oscillations with a period of 3 min show that Ca II grains are formed by acoustic shocks at an altitude of ≈1 Mm above the level $\tau_o = 1$, where τ_o is the optical depth at 500 nm (Carlsson & Stein 1995, 1997). These waves contribute to the heating of the chromosphere, but can only provide a fraction, as most of the internetwork chromosphere, to a filling factor of at least 90% (von Uexküll & Kneer 1995), receives no heat from the 3 min oscillations.

The conflicting results summarized above leave unresolved the temperature structure of the chromosphere (Kalkofen et al. 1999; Kalkofen 2001; Ayres 2002). However, the physical conditions of the photosphere and the lower chromosphere are much better constrained by observations than those of the upper chromosphere and the interface to the transition region. Observations of the H I Lyman continuum formed close to this interface might thus be helpful in improving our understanding. The SUMER spectrometer (Wilhelm et al. 1995) performed detailed measurements of the hydrogen continuum in many regions of the solar atmosphere over the last six years. The analysis of such data obtained in quiet-Sun areas will be the main topic of this study[4].

2. Instrumentation, observations and data handling procedures

The SUMER spectrometer provides us with the opportunity to observe the H I Lyman continuum over a wide wavelength range and with high spatial resolution in network lanes and internetwork areas. This is made possible by the high stray-light suppression of the SUMER instrument, the low background level of the detectors, and the fact that detector B covers the range from 66 nm to 150 nm in the first order of diffraction. The lower limit on the potassium bromide (KBr) photocathode is 67.2 nm. The shortest wavelength observable with detector A in first order is 78 nm (and the longest 161 nm). The angular resolution element (one pixel) of the detectors is approximately 1″ along the slit. For most quiet-Sun observations, slits with a width of 1″ have to be used, but in some ranges of the short-wavelength Lyman continuum the 4″× 300″ slit can be employed to improve the counting statistics within the internetwork areas. The investigation of these very dark regions – the main topic of this contribution – is rather demanding and requires carefully designed observational sequences, which utilize the SUMER capabilities to the fullest extent. Table 1 summarizes the relevant observations, which will be described here in some more detail as observational Sequences 1 to 5:

1. Reference spectra in quiet-Sun regions near the centre of the disk were recorded with detector B late in 1996. These spectra provide the widest wavelength coverage of the H I Lyman continuum and the emission lines in this range, but have the disadvantage that only small areas (0.7 Mm × 84 Mm) of the Sun (corresponding to the 1″× 120″ slit) are seen, with a sampling time of 115 s. Consequently, the results are strongly influenced by temporal variations of the spectral radiance, L_λ, in particular in network lanes. Summing all four quiet-Sun spectra available improves the situation considerably. On the other hand, it is clear that the sampling times are too long for any chromospheric oscillation studies. Note that the reference spectra require a scan of the spectrometer band.
2. On 8 February 1998, a long-duration observation was performed of the O IV and Ne VIII lines between 77 nm and 79 nm together with the Lyman-continuum background. Here we consider the continuum results in detail because the data are of specific interest. They were obtained with twice the standard telemetry rate of SUMER, i.e., 21 000 bits per second, half of which was provided by the Coronal Diagnostic Spectrometer (CDS) (Harrison et al. 1995) for this purpose. This made possible a high cadence with sampling times of 33.5 s and a good spectral coverage. In addition, a special solar rotation compensation scheme was used with the smallest available step width of 0.38″ every 137.4 s. Since the step width was only about one third of the slit width the transitions were very smooth, and this sequence thus has an excellent pointing stability with respect to a given region on the Sun.
3. Three high-cadence runs with transmission to the ground of all the data recorded by the full detector array – originally meant as observing sequence for explosive events in a wide range of formation temperatures – are very useful for studying fast temporal variations of the emission lines in the wavelength range from 75 nm to 79 nm and of the corresponding portion of the Lyman continuum. In particular, the observations of the internetwork regions benefit

[3] The brightness temperature at 137 mm found by SUMER above a sunspot was 4200 K (calculated from Curdt et al. 2001).

[4] All SUMER data acquired are in the public domain and can be obtained from the SOHO Archive as FITS files (`http://soho.nascom.nasa.gov/data/catalogues/main.html`) or from the SUMER Image Database as IDL^R restore files (`http://www.linmpi.mpg.de/english/projekte/sumer/FILE/SumerEntryPage.html`).

Table 1. Selected H I Lyman-continuum and emission-line observations of quiet-Sun regions with SUMER/SOHO.

Sequence Date	Time (UTC)	Duration D/min	Cadence[a] C/s	Wavelength λ/nm	Slit Detector[c]	Pointing[b] y, x, μ	Remarks
1						$y = 0''$; $\mu \approx 1.00$	Reference spectra of H I
11 Oct. 1996	05:16			67.2		$x = 3''$ to $9''$	Lyman continuum & high
17 Oct. 1996	05:32	38	115	to	$1''\times 120''$	$x = 0''$	members of Lyman series
28 Oct. 1996	03:57		(115)	93.5	B	$x = 0''$	averaged over internetwork
12 Nov. 1996	09:48					$x = 0''$	or network areas
2							Four 50-pixel windows of
08 Feb. 1998	17:10	438	34.4	77.0	$1''\times 300''$	$y = 0''$	continuum & O IV, Ne VIII;
			(33.5)	78.0	B	$x = 0''$ to $75''$	high telemetry rate;
				78.8		$\mu \approx 1.00$	special rotation tracking;
				79.0			$1.032''$ per pixel, 708 km/$''$
3							Full detector; continuum
16 Nov. 1996	06:48	6.5	30.0	75.0	$4''\times 300''$	$y = 560''$	& emission lines;
	09:14	6.5	(30.0)	to	B	$x = 0''$	memory: 4.3 MB[d];
	11:41	6.5		79.0		$\mu = 0.69...0.91$	$1.033''$ per pixel, 710 km/$''$
4				79.4			Five 50-pixel windows;
13 Nov. 2001	06:29	22	43.0	81.2	$1''\times 300''$	$y = 650''$	use of grating mechanism;
			(15.0)	82.3	A	$x = 0''$	79.4 nm: $1.031''$ per pixel;
				89.3		$\mu = 0.58...0.86$	90.9 nm: $1.019''$ per pixel;
				90.9			711 km/$''$; memory: 5 MB
5							Continuum &
10 Jun. 1999	12:11	241	150	70.9	$1''\times 300''$	$-233''$ to $-533''$	O III, Mg IX lines;
			(150)	70.3	B	$-391''$ to $-499''$	raster step width: $1.14''$;
				70.6		$\mu = 0.64...0.88$	$1.039''$ per pixel, 729 km/$''$

[a] Sampling times in parentheses.
[b] x: positive towards west, y: positive towards north (both from disk centre); $\mu = \cos\vartheta$, where ϑ is the heliocentric angle.
[c] All observations in first order of diffraction.
[d] 1 MB = 1×10^6 bytes.

from the use of the wide slit as it increased the throughput of the instrument by a factor of four without adverse effect on the continuum measurements. As a consequence, the signal was a factor of 30 above the detector noise, even in the darkest regions. The available telemetry rate and the size of the SUMER data memory limit the duration of each run to about 6.5 min.

4. In November 2001, a fast spectral scan of the Lyman continuum from 79 nm to 91 nm was obtained by moving the grating scan and focus mechanisms back and forth every 43 s. The actual sampling time was 15 s for three simultaneously exposed windows at the short-wavelength side and another 15 s for two windows near the Lyman edge. The movements of the mechanisms lasted 2×6.5 s per cycle. This mode had never been used before during the past SOHO mission duration because of the many movements involved. After 22 min the capacity of the instrument data memory was exceeded and the run was automatically terminated. Near the centre of the disk there was no quiet-Sun region present at that time, and the pointing selected for this sequence had the largest separation from disk centre of all runs discussed here. The heliocentric angle of the centre of the slit was $\vartheta \approx 42^\circ$ and $\mu = \cos\vartheta \approx 0.75$. To assess the significance of this pointing, it should be noted that Warren et al. (1998) found no apparent centre-to-limb variation of the radiance at (91.00 ± 0.05) nm, whereas Noyes & Kalkofen (1970) derived typical centre-to-limb variations from OSO-4 (Orbiting Solar Observatory) observations that show some limb darkening above 82.5 nm and a relative limb brightening of ≈20% at 66.7 nm. In all cases, no effect would be expected for $\mu \geq 0.6$, and thus Sequences 3 to 5 will be compared to Sequences 1 and 2 without adjustments of the radiances.
5. A study of the spectral radiance of the Lyman continuum at short wavelengths (near 70.9 nm) and its relation to transition-region and coronal emission lines was performed on 10 June 1999. A raster scan of the spectrometer slit covered an area of approximately 100 Mm × 210 Mm, including a small coronal hole on the disk surrounded by quiet-Sun regions. This scan built up images of this area, but, of course, the sequence did not yield any information on oscillations.

The focussing requirement of the SUMER grating in Wadsworth mount leads to a change of the plate scale on the detector as a function of wavelength. The seasonal variation of the Sun-SOHO distance introduces yet another scale change. Both scales are listed in the last column of Table 1 for Sequences 2 to 5.

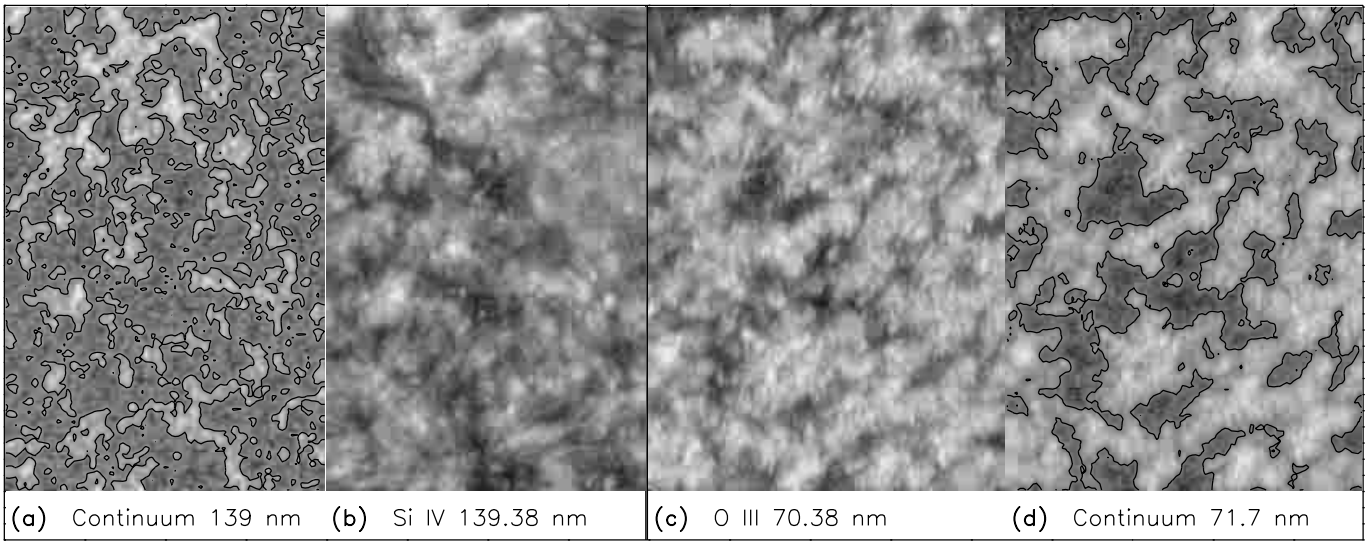

Fig. 1. Structure of the chromospheric network at different brightness or formation temperatures (T_B or T_F) on 11 and 12 June 1999. **a)** The network lanes are composed of small bright dots in the Si I continuum at 139 nm. Isolated bright dots can also be seen in internetwork areas. A contour at the level of the mean between the maximum and minimum brightness (smoothed over 2×2 pixels) is superimposed on the radiance map. These observations are similar to those of Cook et al. (1983) and Foing & Bonnet (1984) who found small network and internetwork bright points near 160 nm with HRTS and the Transition Region Camera (TRC). **b)** At $T_F \approx 74\,000$ K, the formation temperature of the Si IV line at 139.38 nm, the structure of the network lanes (simultaneously recorded with the 139 nm continuum from 04:06 to 04:22 UTC on 11 June 1999; size of area: ≈144 Mm × 220 Mm) is much more pronounced. Small loop-like features straddle the lanes and some faint arches are crossing the internetwork regions. **c)** In the O III 70.38 nm line, the general network structure is very similar to that of Si IV, although the formation temperature is higher by about 30 000 K. (Note that the O III and 71.7 nm continuum scans are obtained on the following day between 18:01 and 23:54 UTC; size of area: ≈160 Mm × 220 Mm.) **d)** The structure seen in the H I Lyman continuum at 71.7 nm ($T_B \approx 7000$ K) is however very different from that of the Si I continuum ($T_B \approx 4500$ K) and resembles those of transition-region lines. The contour map in this panel (obtained in the same manner as for panel **a**) outlines much broader and more continuous network lanes, and shows fewer bright points in the internetwork areas.

The raw telemetry data have been treated with the help of standard SUMER data-handling routines documented in and available from SolarSoft (SSW):

(a) Decompression (`decompress.pro`).
(b) Flat-field correction with the closest flat-field image available (`sum_flatfield.pro`), except for Sequence 1 that is integrated along the slit over 110 pixels.
(c) Deadtime correction (`deadtime_corr.pro`).
(d) Image distortion correction (`destr_bilin.pro`).
(e) Gain-depression correction (`local_gain_corr.pro`).
(f) Radiometric calibration (`radiometry.pro`) in its latest version (`epoch_9`) to get the spectral radiance, L_λ, in physical units.

In many cases the deadtime and local-gain corrections introduced only very small adjustments, but nevertheless all corrections were applied to all data files.

3. Analysis

3.1. Network structure

Before a detailed analysis of the H I Lyman-continuum observations will be presented it is useful to show in Fig. 1 the chromospheric network structure as seen in two continua and two emission lines by the SUMER spectrometer, with a spatial resolution element of typically 1″. In particular, the different appearance of the network in a the Si I continuum and d the H I continuum is worth noting. The morphology of the network lanes observed at various formation temperatures of the emission has been the major topic of recent papers using SOHO observations (Patsourakos et al. 1999; Feldman et al. 2001). The width of the network boundaries found was ≈8 Mm (10″ to 12″) for temperatures between $T_F = 30\,000$ K and 400 000 K, with rapid spreading and disintegration at higher temperatures. With lower spatial and spectral resolution the network of the quiet Sun has been observed in the same wavelength ranges and with qualitatively similar results by Skylab (Reeves et al. 1974; Reeves 1976). The maximum contrast between network and internetwork regions occurred at 160 000 K.

It would be ideal if the observed plasma distribution could be related to small-scale magnetic-field configurations of the quiet Sun. A schematic sketch of network fields was first provided by Noyes (1967), based on spectroheliographic measurements of velocities in the photosphere and the lower chromosphere (Leighton et al. 1962; Simon & Leighton 1964). These measurements gave average supergranulation cell sizes of 32 Mm, lifetimes of up to 20 h, and peak horizontal and vertical velocities in the photosphere of ≈0.4 km s^{-1} and ≈0.1 km s^{-1}, respectively. However, even now there is no general agreement on a magnetic-field configuration of the chromospheric network. Gabriel's (1976) canopy model augmented by network loops (Dowdy et al. 1986) probably is still the best description available, although many questions remain unanswered. In this model, the internetwork regions are relatively

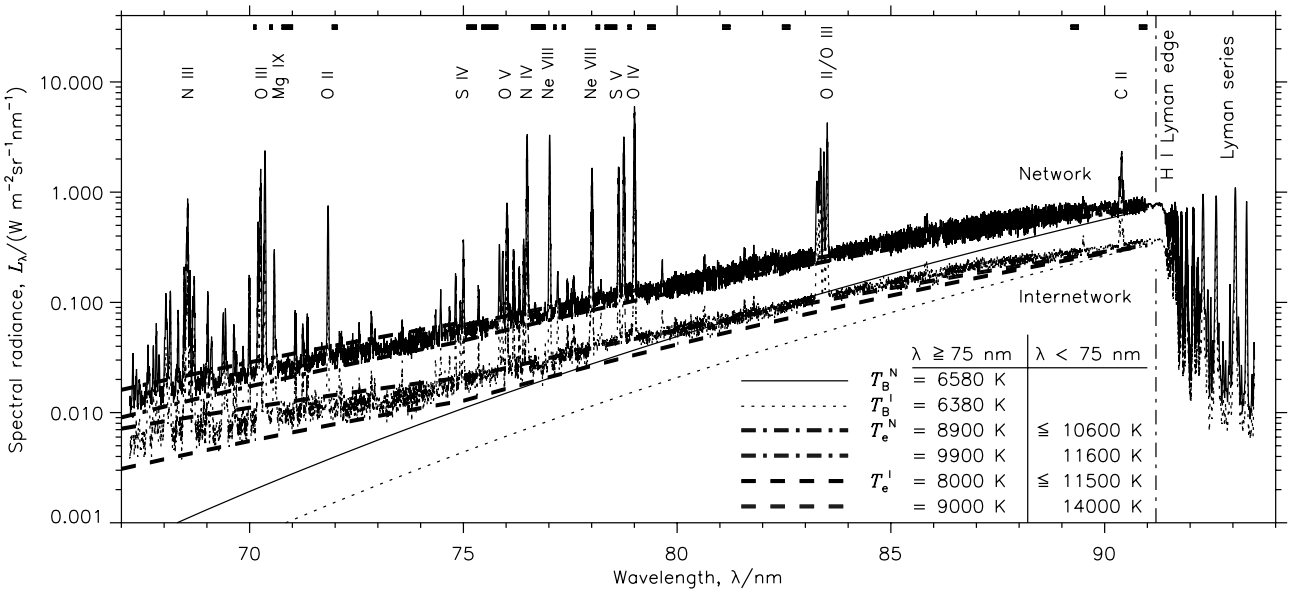

Fig. 2. Quiet-Sun observations of the H I Lyman continuum averaged over relevant sections of four SUMER detector B reference spectra taken on the KBr photocathode. The measurements were made near the centre of the disk in late 1996 (Sequence 1). The spectra are integrated along the slit, but separated into network and internetwork sections. Planck functions with brightness temperatures, T_B^N and T_B^I, are matched to the spectral radiances at the H I Lyman-continuum head. The slopes of the continuum have been used to define kinetic electron temperatures, T_e, and departure coefficients (for details see text) both for the network and internetwork spectra as upper and lower estimates each. Several prominent emission lines and multiplets are identified. The wavelength bands in which more detailed H I Lyman-continuum observations have been performed in this study are marked at the top of the diagram by black bars.

devoid of magnetic fields, and in many chromospheric studies the internetwork is indeed characterized as "largely nonmagnetic" or as a region where magnetic fields are dynamically unimportant (see, for instance, recent reviews by Kalkofen et al. 2003; Ulmschneider & Kalkofen 2003).

In this context, it should be pointed out that in Fig. 1a there are many bright points in internetwork regions, too. Using HRTS data, these bright points have been studied by Hoekzema et al. (1997), who found that they are statistically related to the acoustic shock dynamics in the internetwork. Foing & Bonnet (1984) concluded, based on their TRC observations, that the bright network elements (≤1 Mm) are related to magnetic-flux concentrations, but that the corresponding internetwork brightenings are most likely caused by a process which also produces the H and K grains. If some of the bright points were related to magnetic-field concentrations, as the network bright points are, a re-assessment of the field-free internetwork assumption would be necessary. However, the oscillation frequencies observed in the internetwork chromosphere suggest that magnetic fields play no rôle in the waves observed in grains (Kalkofen et al. 1999).

In a review on small-scale solar magnetic fields, Solanki (1993) discussed many aspects of "inner network fields" and Rosenthal et al. (2002) have very recently found in numerical simulations that waves might be influenced by such fields. The "magnetic shadows" detected in internetwork regions adjacent to network lanes have been interpreted as a direct consequence of such an interaction (Judge et al. 2001; McIntosh et al. 2001; Cally 2001).

The radiation of the H I Lyman continuum, which is formed in the upper chromosphere (cf., Biermann 1948; VAL81) near the interface to the transition region, is relatively strong in network lanes (de-focussed images of the H I continuum at 88 nm are in fact being used to acquire the SUMER flat-field exposures; Schühle et al. 1998), but is up to a factor of ten weaker in the internetwork (cf., Fig. 9a for an example at 90.90 nm). To extract useful information from the faint internetwork radiation it is, therefore, of extreme importance to analyse both regimes separately.

3.2. Spectral shape

The wavelength range of the H I continuum that can be scanned by SUMER in first order of diffraction is shown in Fig. 2. The measurements are sorted into network and internetwork regions along the slit and averaged over four quiet-Sun reference spectra. The selection criterion – applied to the actual setting of the spectrometer band and pairs of pixels – was $L_\lambda^N \geq (L_\lambda^{max} + L_\lambda^{min})/3 > L_\lambda^I$, which led to about the same number of pixel pairs in both bins (N: network; I: internetwork). Figure 3 demonstrates as an example the result of such a scheme. A strong network lane was intersected by the slit at the pixel positions $s = 35$ to 55. A narrower lane can be seen near $s = 20$. Both lanes slowly move to higher pixels positions as a consequence of the solar rotation. Some weak network activities were encountered at $s = 5$ and 90. Inspection of the other spectra gave similar results, but no systematic shift of the lanes was observed for the spectrum of 11 October 1996, because the SUMER rotation compensation had been activated at that time (cf., Table 1). It can be concluded that the selection criterion provides a reasonable separation into network and internetwork regions. The spectral radiances at the Lyman edge

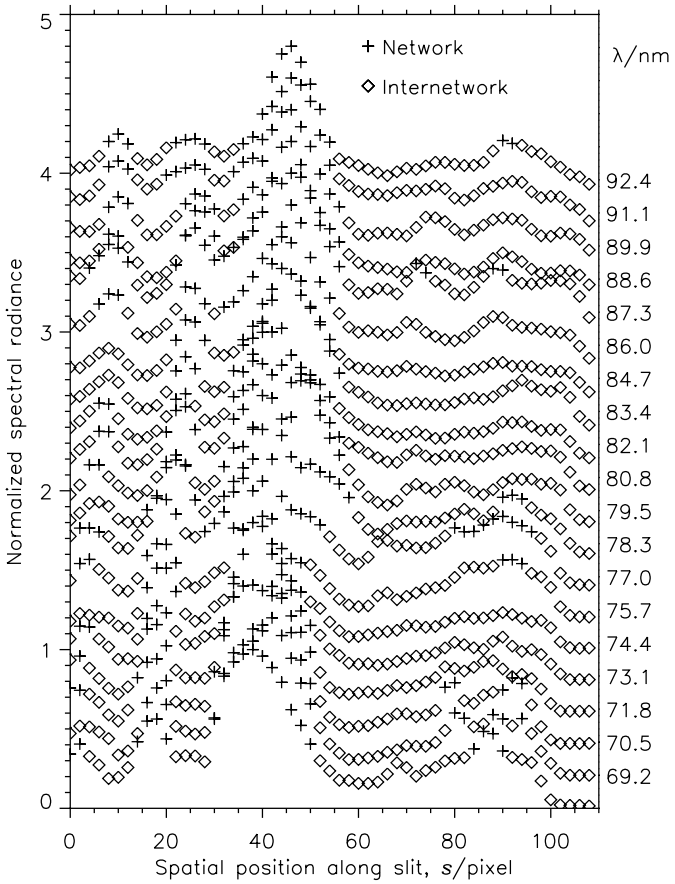

Fig. 3. Normalized spectral radiances along the slit are shown for the 20 exposures on 17 October 1996 that have been used in the compilation of Fig. 2. The central wavelengths of the exposures (successively shifted up by +0.2 for display purposes) are given in the right margin. Applying the selection criterion of Sect. 3.2 the data are sorted into network and internetwork points.

(λ_H = 91.2 nm) in Fig. 2 define brightness (or radiation) temperatures $T_B^N(\lambda_H) = 6580$ K and $T_B^I(\lambda_H) = 6380$ K by applying Planck's law

$$L_\lambda = B_\lambda(T_B) = \frac{2\,h\,c_0^2}{\lambda^5}\left[\exp\left(\frac{h\,c_0}{\lambda\,k\,T_B}\right) - 1\right]^{-1}$$

for a wavelength of $\lambda = \lambda_H$, where h is the Planck constant, c_0 the speed of light in vacuum, and k the Boltzmann constant.

The slopes of B_λ(6580 K) and B_λ(6380 K) versus wavelength are much steeper than those of the measured continua, implying departures from LTE in which the ground state of H I is overpopulated relative to its equilibrium value in terms of the Saha equation. Reasonable fits to the slopes in the wavelength range from 91.2 nm down to 75 nm can be achieved with colour temperatures between T_C^N = 8900 K and 9900 K, and T_C^I = 8000 K and 9000 K. The colour temperature of the Lyman continuum can be interpreted as the electron temperature, T_e, of the plasma (cf., Brekke & Kjeldseth-Moe 1994b). At shorter wavelengths the observed spectral radiances are higher than one would expect from an extrapolation of the slopes at longer wavelengths, both for the network and the internetwork. For the latter it has to be checked whether detector background counts could cause the excess; as Fig. 11a indicates, this cannot be ruled out.

However, the network spectral radiance is far above the detector background and yet deviates from the colour temperature fit valid for $\lambda \geq 75$ nm. Moreover, the sunspot spectrum of the SUMER spectral atlas (Curdt et al. 2001) shows that radiances as low as 0.002 W m^{-2} sr^{-1} nm^{-1} can be measured near 70 nm even with the 0.3″ wide slit. Another possibility – a systematic deviation of the response function used for the radiometric calibration (Wilhelm et al. 2002) – is unlikely since the deviations in the network and internetwork are different. Furthermore, Fig. 3 of VAL81 shows the same trend for OSO-6 and Skylab data. It can therefore be concluded that the excess may be real and indicates that this portion of the H I continuum is formed on the steep temperature rise of the upper chromosphere (cf., Fig. 1 of VAL81). But while a change in the slopes of $T_e^I(\lambda)$ and $T_e^N(\lambda)$ could be a plausible consequence of the steep temperature profile and rapid variation of its gradient in the upper chromosphere and lower transition region, the sudden change at 75 nm is surprising in view of the smooth variation of the photoionization cross-section of hydrogen with wavelength and the smoothing properties of radiative transfer. It is interesting to note that in this wavelength range the internetwork temperatures, T_e^I, implied by Fig. 2 are *higher* than those of the network, with the qualification that the temperatures T_e^I are upper limits since they might be affected by background counts.

Spectra acquired by the Harvard spectroheliometer on OSO 4 were analyzed by Noyes & Kalkofen (1970) who modelled disk-integrated observations with a spectral resolution element of 0.32 nm and obtained T_B = 6450 K and T_e = 8300 K, where T_e is the kinetic temperature of the electrons at optical depth unity at the Lyman edge. These brightness and electron temperatures lie between the brightness and colour temperatures for the internetwork and network regions obtained with SUMER. The limited spectral resolution of the OSO-4 observations restricted the useful range of the Lyman continuum to values between 91 nm and 79 nm, which is relatively free of prominent emission lines. The high density of spectral lines below 79 nm prevented an unambiguous determination of the spectral radiance of the continuum at short wavelengths. The OSO-4 results gave a dilution factor of 200 for the black-body radiation at the head of the Lyman continuum, which could be identified with the departure coefficient, b_1, in

$$S_\lambda = B_\lambda(T_e)/b_1$$

where b_1 is the factor by which the density in the ground state of hydrogen departs from its thermodynamic equilibrium value in terms of the Saha equation (cf., Menzel 1937; Pottasch & Thomas 1959), and S_λ is the source function for negligible stimulated emission. The emergent spectral radiance in general closely matches the source function at optical depth unity ($\tau_\lambda = 1$) in the Lyman continuum

$$L_\lambda = S_\lambda(\tau_\lambda).$$

This is also the case in a time-dependent medium, as in the dynamical wave model of Carlsson & Stein (1994; see their Fig. 4) even though the amplitude of temperature fluctuations significantly exceeds that observed with SUMER.

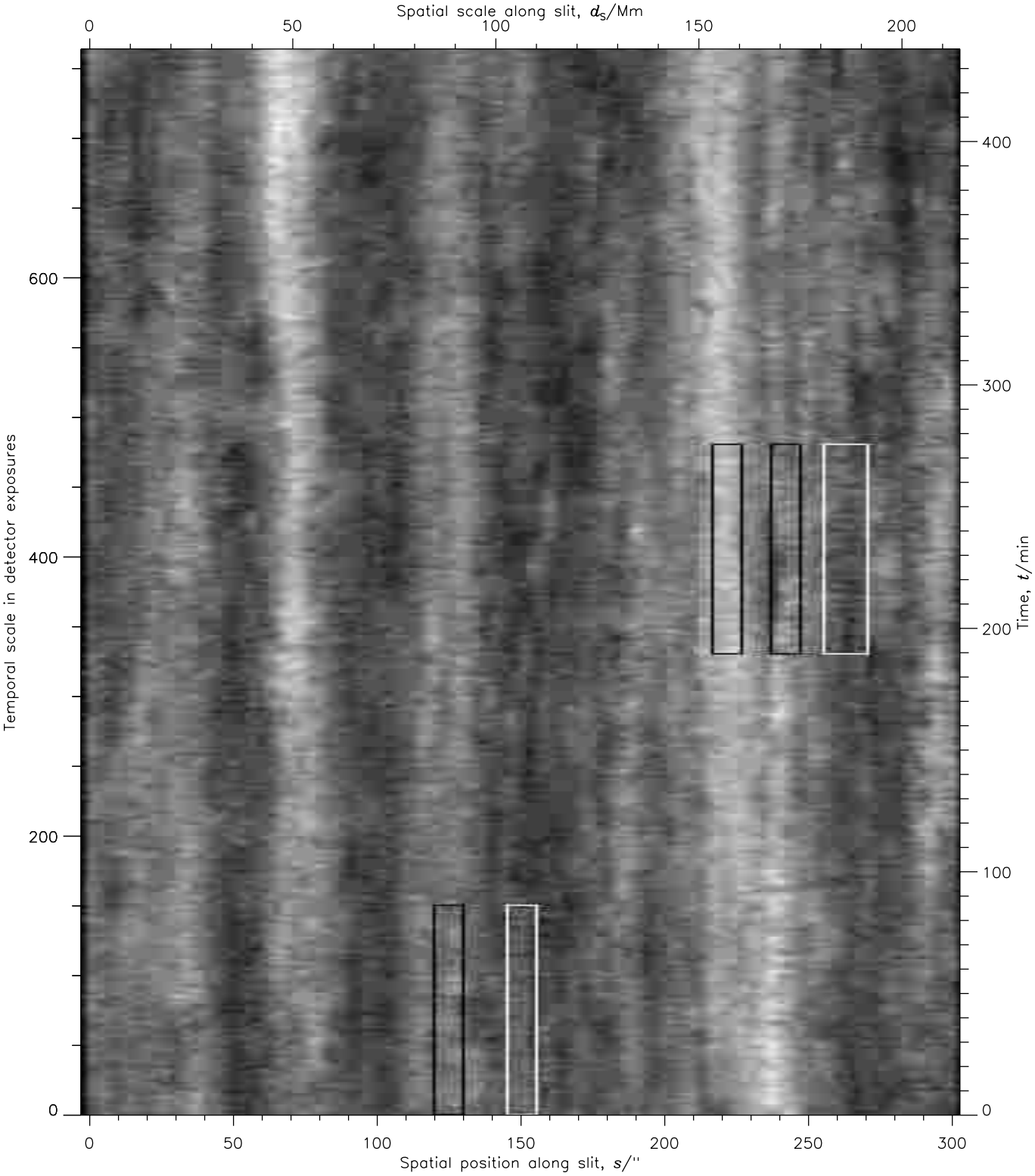

Fig. 4. Space-time chart of the brightness temperatures of the quiet-Sun chromospheric network near the centre of the solar disk on 8 February 1998 (Sequence 2). Several bright network lanes and dark internetwork regions were traversed by the 1″ × 300″ slit. (North is towards decreasing position numbers. The dark margins near 0″ and 300″ show detector pixels not illuminated by the slit.) The spectral ranges covered in this diagram include the H I Lyman continuum next to the emission lines Ne VIII at 77.04 nm, 78.03 nm and O IV at 78.77 nm, 79.02 nm. The minimum brightness temperature was T_B = 6400 K and the maximum 7360 K, with a mean of 6830 K. Pronounced internetwork oscillations can only be seen between spatial positions s = 145″ and 155″ from t_0 = 0 min to t_1 = 85 min and between positions s = 253″ and 268″ from t_0 = 189 min to t_1 = 275 min. These regimes are enclosed by white frames, whereas some typical network activity is marked in black.

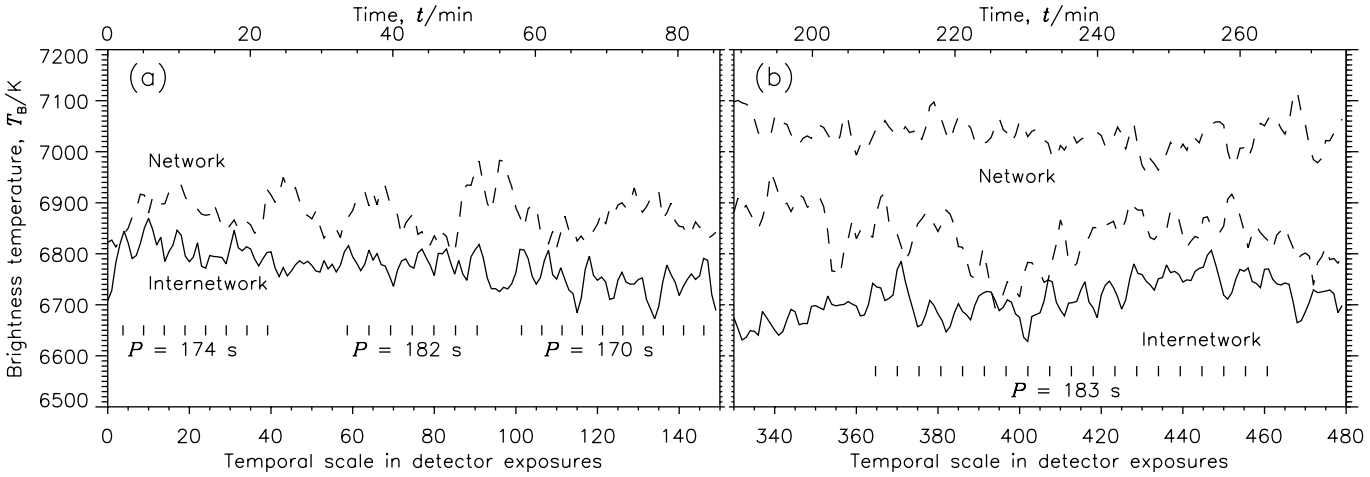

Fig. 5. Amplitude diagrams of quasi-oscillatory chromospheric brightness variations seen in the H I Lyman continuum displayed in Fig. 4. **a)** Internetwork oscillations (solid line) are shown near spatial position $s = 150''$ in comparison with adjacent network activity (dashed line) close to spatial position $s = 125''$. **b)** Oscillations in an internetwork region were also present near position $s = 260''$. Variations near positions $220''$ and $240''$ in bright and intermediate network lanes are included for comparison. Some markers indicating periods, P, from 170 s to 183 s are plotted below the internetwork variation to guide the eye.

The SUMER spectra yield $b_1^{\rm N} \approx 500$ and $b_1^{\rm I} \approx 150$ for $\lambda \geq 75$ nm and the lower temperature estimate in Fig. 2, both with a relative uncertainty of 25%, caused by the uncertainty of the radiometric calibration. Again the SUMER values bracket the OSO-4 result. It has to be noted though that the method is inherently inaccurate since the temperature changes rapidly with depth in the formation region of the H I continuum, as was pointed out in VAL81. The uncertainty in the calibration must be kept in mind in judging the validity of the breaks in the temperature assignments at 75 nm in Fig. 2 since, as mentioned before, the smooth variation of the photoabsorption cross-section as well as the properties of radiative transfer would tend to give a gradual variation of the colour temperature even if the solar temperature changed abruptly.

Below 75 nm the departure coefficients are much larger than at longer wavelengths, namely, $b_1^{\rm N} \approx 1.6 \times 10^4$ and $b_1^{\rm I} \approx 2.2 \times 10^5$, where $b_1^{\rm N}$ is now *smaller* than $b_1^{\rm I}$. Finally, it should be mentioned that the spectral radiances at the Lyman edge in Fig. 2 correspond to model D of VAL81 for network observations and to model B for the internetwork.

3.3. Temporal variations

The sequence executed on 8 February 1998 has provided more than 7 h of uninterrupted observations of the Lyman continuum near 78 nm, as shown in Fig. 4. This sequence has been described by Gouttebroze et al. (1999) as far as the transition-region and coronal lines are concerned. The $1'' \times 300''$ slit crossed several prominent network lanes and internetwork regions. Although there were many changes of the small-scale structure, the basic network configuration was stable during the duration of this run. Oscillatory variations of the radiance in network lanes appear to be quite common, but only two clear, long-lasting episodes could be found in internetwork regions. Shorter brightenings can be observed there as well, some of them even of periodic nature, but about 50% of the space-time regime in the internetwork is free of them. The identified episodes are highlighted by white frames in Fig. 4 and are shown as amplitude displays in Figs. 5a and 5b together with adjacent network activities (black frames in Fig. 4).

The temporal variations of the H I Lyman continuum and the C I continuum near 104.3 nm are quite dissimilar, as can best be seen by comparing our Fig. 4 with Fig. 2 of Wikstøl et al. (2000) where a distinct oscillatory behaviour with periods of 100 s to 200 s is a characteristic feature of all internetwork regions. Hansteen (1997) compared space-time plots of the radiance in the far H I Ly α wing with those of the Lyman continuum and found no oscillations in the continuum, whereas they were pervading the plot of the Ly α wing.

This suggests that only the strongest acoustic events discussed by Hoekzema et al. (2002) can also be seen in the Lyman continuum. It is consistent with the fact that in co-aligned observations of the Vacuum Tower Telescope (VTT) (Ca II K) and SUMER (emission lines with low formation temperatures) not many events can be traced from the middle chromosphere to the upper chromosphere and the transition region (Steffens et al. 1997b). Similarly, Curdt & Heinzel (1998) and Curdt et al. (1999) could follow oscillatory variations from the lower chromosphere (Ca II K_{2v}) to the upper chromosphere (H I Lyman lines and the continuum) in network regions, but not in internetwork areas.

The short observing sequences of 16 November 1996 are not suitable for studying the oscillatory pattern of the Lyman continuum, but can be searched for strong events that display typical temporal variations. Given the complete spectral, spatial and temporal information available for these runs, the events can then be fully characterized. The 3×13 spectra obtained by integration over the pixels with low signal along the slit are displayed in Fig. 6. They are representing average internetwork spectra. The brightness temperature of the continuum is $T_{\rm B}^{\rm I} \approx 6700$ K in this wavelength range (approximate fit to the bottom spectra). Specifically, $T_{\rm B}^{\rm I} = 6770$ K at 75.45 nm,

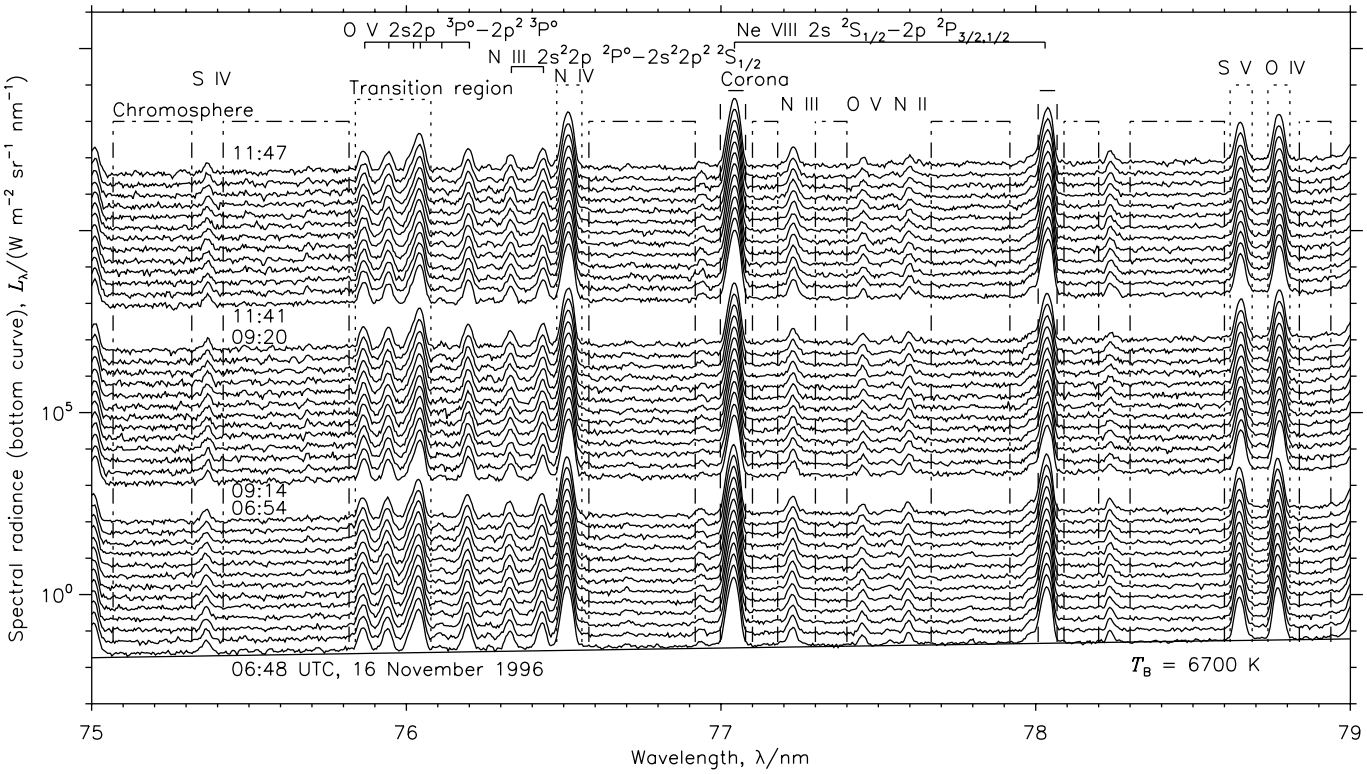

Fig. 6. Spectra of the H I Lyman continuum from 75 nm to 79 nm with prominent lines of the transition region (N II, N III, N IV, O IV, O V, S IV, S V) and the corona (Ne VIII) (Sequence 3). The spectra have been obtained by selecting pixels along the 4″ × 300″ slit with low output signals (representative of internetwork regions) and subsequent integration. Three time periods have been covered in burst modes with a cadence of 30 s generating thirteen spectra each (for details see text). Spectral ranges free of emission lines define the continuum. They are marked by dashed-dotted demarcations and labelled with "chromosphere". In addition, the ranges with transition-region and coronal emission are encompassed by dotted and dashed lines. The spectral radiance for a brightness temperature of T_B = 6700 K is shown in comparison to the bottom curve of the diagram. Later spectra of each burst are successively displaced by a factor of two for display purposes. Note the extremely compressed (logarithmic) scale of the ordinate.

6740 K at 76.80 nm, and 6700 K at 78.60 nm. Strong and weak emission lines are also present in this range, from the transition region (N II, N III, N IV, O IV, O V, S IV, S V) and the corona (Ne VIII). The temporal stability of the spectra is the most impressive result seen in this diagram, although the integration over all internetwork positions and the compressed radiance scale have to be kept in mind.

Integration of the pixels with high signal levels gave a plot (not shown) which looked very similar, with spectral radiances about a factor of two higher in the continuum (yielding brightness temperatures T_B^N = 6990 K at 75.45 nm, 6950 K at 76.80 nm, and 6910 K at 78.60 nm) and a factor of ten for the transition-region lines. The Ne VIII lines did not change significantly. The spectral ranges designated "chromosphere", "transition region", and "corona" in Fig. 6 are shown separately for the first burst observation, now plotted versus the spatial position along the slit in Fig. 7. The other two runs are similar and are not shown because they do not convey any additional information. In Fig. 7, typical internetwork regions are indicated within which some temporal variations are marked by plus signs. They can be followed from the chromosphere to the transition region, but are not or barely visible in the corona. The event near spatial position 190″ was selected for display in Fig. 8a. Events from the other two bursts complete Fig. 8. Quantitative results are given in the first row of Table 2, where the ratio, R_{max}, of the extremes of the maxima during each of the three events is listed, as well as the ratio of the extremes of the radiance integrated over the extension of the event along the slit, R_{total}. The radiances of the chromosphere and the transition region normalized to their minimum values typically increase by factors of 1.2 to 1.4 and brighten in phase, whereas the line radiances of the corona are rather stable, without any obvious phase relationship. The radiance variations of the transition-region lines tend to be larger than those of the Lyman continuum from the chromosphere. Gouttebroze et al. (1999) also found no phase difference between Si I 125.6 nm and Si II 126.0 nm, but did not treat network and internetwork regions separately.

3.4. Wavelength dependence

The temporal variations of the Lyman continuum shown in Fig. 8 as solid lines – resembling 180 s chromospheric brightenings – have been observed near 77 nm. It is of interest to study their wavelength dependence over a wide range of the Lyman continuum. Since the SUMER detectors only cover a spectral window of ≈4.4 nm at any one time, the grating mechanisms had to be used to extend the range to about 12 nm. This

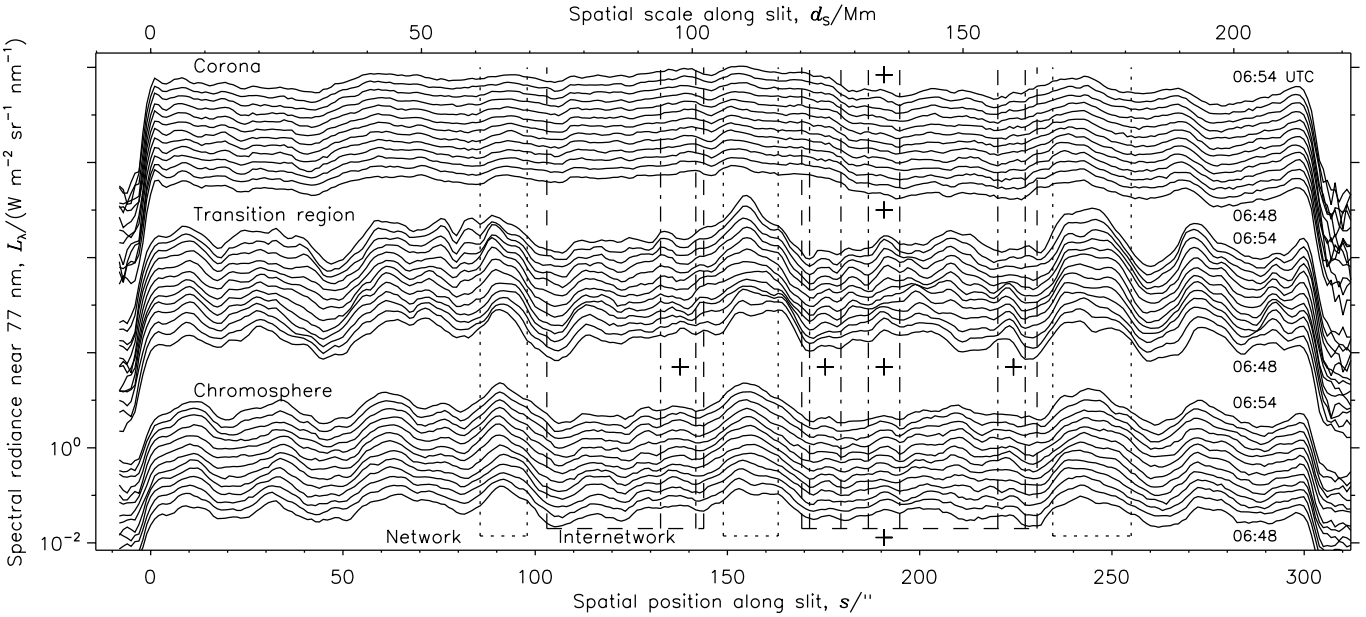

Fig. 7. Plots of the spectral radiances along the slit of chromospheric, transition-region, and coronal emissions (as defined in Fig. 6) for the thirteen exposures obtained during the first burst-mode observation on 16 November 1996. The H I Lyman-continuum radiation of the chromosphere is given in physical units, with a scale valid for the bottom curve (later curves are successively displaced by a factor of 1.5), the line emissions, however, are in arbitrary units. Typical network and internetwork crossings of the slit are marked and some temporal variations of the radiances are highlighted by plus signs in internetwork sections. Some dark pixels on either side of the slit are included in order to document the detector background levels.

is the maximum attainable with detector A, which was in operation during the campaign in November 2001. Five 50-pixel windows (0.22 nm each) centred at (79.4, 81.2, 82.3, 89.3, and 90.9) nm were telemetered to the ground with a cadence of 43 s (cf., Table 1). Figures 9a and 9b display the observations obtained in two of the windows. The data of the other windows look qualitatively very similar and are not shown here. Network and internetwork sections have been indicated. An interesting aspect of these measurements is the trend towards lower radiances near an active region (AR), which suggests that convection is inhibited and hence wave generation is reduced near magnetic-field elements. A similar decrease has been observed in the S VI line at 93.3 nm near AR NOAA 7962 on 12 May 1996 (Wilhelm et al. 1998).

Several brightenings in the internetwork are present in Fig. 9. The one selected for further analysis is marked by plus signs. Its temporal variations at all five wavelengths are plotted in Fig. 10. It is obvious that all variations are very closely correlated with a tendency of larger relative amplitudes at shorter wavelengths in addition to some increase in noise. Numerical results are compiled in Table 2 together with those of November 1996. The November 2001 results (referring to one event) confirm the tendency of larger relative amplitudes with decreasing wavelength, which is a consequence of the greater temperature sensitivity of the source function in the Lyman continuum at shorter wavelength. This result holds for both methods of evaluation ($R_{\max}$ and R_{total}) defined in the previous section. The November 1996 results obviously cannot directly be compared with the other event.

3.5. Coupling between chromosphere, transition region, and corona

The data displayed in Fig. 7 and the corresponding ones obtained during the following two burst observations can be used to determine the coupling between the upper chromosphere, the transition region and the lower corona. To this end, the correlation coefficients of the radiance variations along the slit have been calculated for all three combinations. Calculations were performed using the data of the ensemble of the sets and each individual exposure (in order to get some idea on the variance of the measurements). The results are summarized in the first three rows of Table 3 from which it can be seen that the correlation between the chromospheric variations and those of the transition region is very high (as one would have expected), and that the correlation between the chromosphere and the corona is slightly *higher* than that between the transition region and the corona in all three cases. However, the differences are too small and the standard uncertainties are too large to claim a statistically significant effect.

These findings, therefore, have further been scrutinized with the help of other data sets in Table 1. The sequence of 8 February 1998 can be directly compared with the November 1996 run, because it covers the same wavelength range. In addition to the analysis of the continuum presented in Fig. 4, corresponding evaluations of the O IV lines (representative of the transition region) and the Ne VIII lines (representative of the corona) had to be performed before the correlation coefficients could be determined as given in Table 3. These calculations confirm the results of November 1996, but again do not allow

Table 2. Radiance ratios, R_{max}, R_{total} (with some standard uncertainties obtained from the counting statistics in parentheses), observed during brightening events in quiet-Sun internetwork regions.

Date	Wavelength λ/nm	Spatial resolution element $\Delta x \times \Delta y$/Mm^2	Brightenings of the continuum R_{max}	R^a_{total}
16 Nov. 1996	77.00	2.8×0.7	1.51 1.34 1.41	1.44 1.18 1.22
13 Nov. 2001	79.40	0.7×4.2	1.98 (0.30)	1.69 (0.19)
	81.15	0.7×2.8	1.55 (0.25)	1.42 (0.12)
	82.55	0.7×2.8	1.67 (0.23)	1.45 (0.12)
	89.30	0.7×1.4	1.71 (0.14)	1.32 (0.04)
	90.90	0.7×1.4	1.59 (0.11)	1.28 (0.03)

[a] Averaged over nine to twelve spatial pixels.

Table 3. Correlation coefficients (with standard deviations) along the SUMER slit in quiet-Sun regions.

Date	Time (UTC)	Chromosphere/TR[a]	Chromosphere/corona	TR/corona	Remarks
16 Nov. 1996	06:48	0.92 (0.02)	0.57 (0.04)	0.51 (0.03)	continuum near 77 nm (Chr.),
	09:14	0.91 (0.03)	0.65 (0.03)	0.63 (0.03)	N IV, O IV, O V, S V (TR),
	11:41	0.90 (0.02)	0.30 (0.04)	0.27 (0.04)	Ne VIII (Corona).
	06:48	0.87 (0.05)	0.72 (0.06)	0.62 (0.09)	Network
	06:48	0.72 (0.07)	0.24 (0.06)	0.09 (0.13)	Internetwork
08 Feb. 1998	17:10	0.86 (0.01)	0.48 (0.09)	0.44 (0.09)	78 nm, O IV, Ne VIII
	17:10	0.79	0.41	0.38	Network
	17:10	0.58	0.28	0.26	Internetwork
10 Jun. 1999	12:11	0.86 (0.03)	0.61 (0.13)	0.45 (0.11)	coronal hole (CH) included
	12:11	0.83	0.47	0.36	71.7 nm, O III, Mg IX (w/o CH)
	12:11	0.62	0.43	0.09	Network (w/o CH)
	12:11	0.78	0.37	0.20	Internetwork (w/o CH)

[a] Transition region.

a clear statement on the connection between the corona and the other two regions. It should be mentioned that Patsourakos & Vial (2002) have analysed the same observational sequence to demonstrate the intermittency in the O IV radiance variations.

The coupling of the corona with the lower solar atmosphere can also be investigated with data acquired on 10 June 1999 at shorter wavelengths. In Figs. 11a to 11c the H I continuum near 70.9 nm, the O III lines near 70.3 nm, and the Mg IX 70.60 nm line are shown for a raster scan of a quiet-Sun area containing a small coronal hole. Calculations as described for the 1998 data lead to correlation coefficients that are also listed in Table 3. For these calculations, the area of the coronal hole was either included or not included. In the latter case, the data set was treated as a whole so that no estimates of the uncertainties could be obtained. They indeed seem to reveal a closer relationship between the chromosphere and the corona than between the transition region and the corona. It is interesting to note that the coronal hole outlined in Fig. 11c (corona) can readily be identified in Fig. 11a (chromosphere), but only with difficulty in Fig. 11b (transition region). Outside the coronal hole, the spatial structure of the Mg IX emission is fundamentally different from that of the O III lines, which is a high-resolution confirmation of much earlier observations made on Skylab (Reeves et al. 1974; Reeves 1976).

In calculating the above correlation coefficients, the network and internetwork regions crossed by the slit were not treated separately, in contrast to the evaluations in the previous sections. This procedure was motivated by the fact that the most pronounced spatial radiance variations were related to the network/internetwork structure. Nevertheless, in the context of this study, it might be of interest to compute the corresponding correlation coefficients for internetwork and network sections individually. This has been done for some of the data sets, and the results are also listed in Table 3. Not surprisingly, the coefficients so obtained show much more scatter, but qualitatively agree with the values found from the combined evaluations.

The Lyman-continuum data of 10 June 1999 have also been used to determine the brightness temperatures at ≈70.9 nm outside the coronal hole as T_B = 7750 K (maximum), 7410 K (network), 7250 K (mean), 7140 K (internetwork), and 6790 K (minimum). The temperature in the coronal hole was ≈6800 K. The last two values were very near the detector background level and have to be considered upper limits.

4. Discussion

An overview of the H I Lyman-continuum observations analysed in Sect. 3 can best be obtained by plotting in Fig. 12 the brightness temperatures for various conditions as functions of

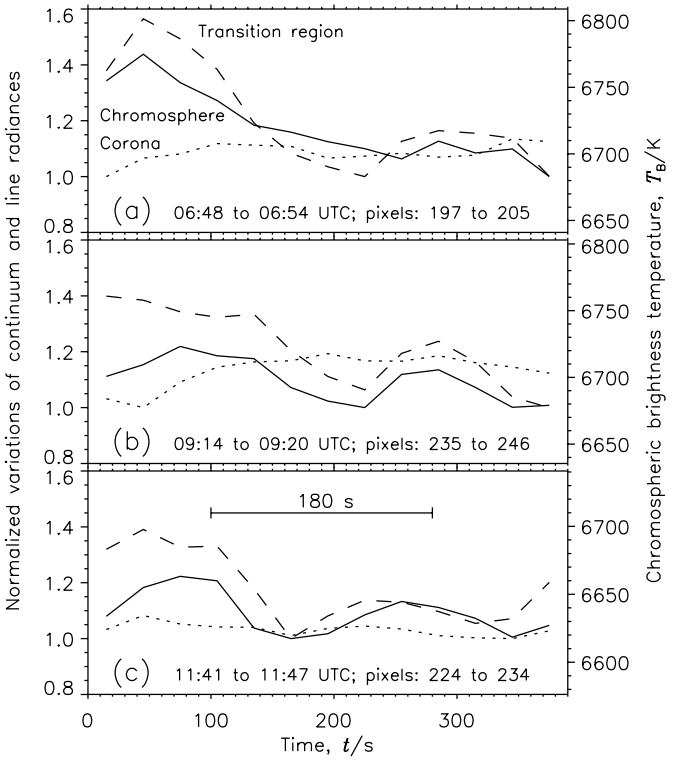

Fig. 8. Temporal variations of the radiance (normalized to the minimum values) for typical brightenings with temporal separations of about 180 s in internetwork regions. The observations were made on 16 November 1996 (Sequence 3) and have been integrated over 9 to 12 spatial pixels as indicated. Solid lines represent chromospheric H I Lyman-continuum emission near 77 nm (brightness temperatures are shown on the right-hand side), dashed lines stand for transition-region and dotted lines for coronal emissions. **a)** The event in the upper panel occurred during the interval displayed in Fig. 7. **b), c)** The other events stem from the following two burst-mode observations.

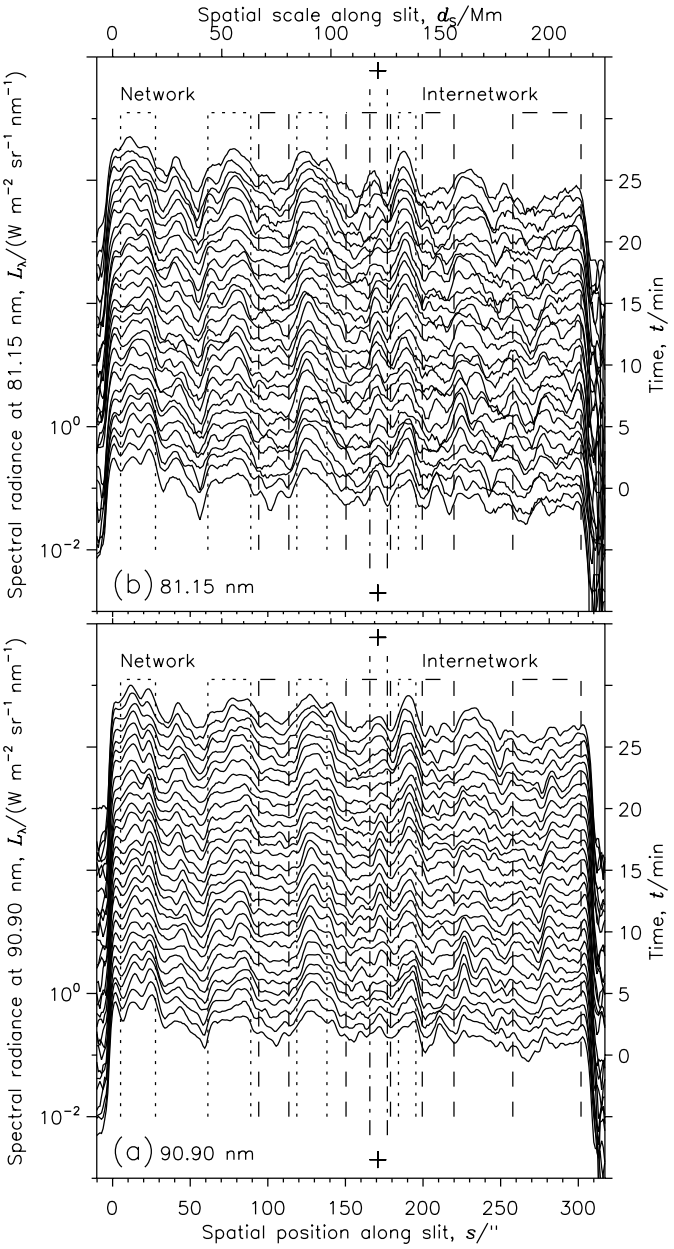

Fig. 9. H I Lyman-continuum observations (Sequence 4). **a)** Measurements near the Lyman edge are smoothed over two spatial pixels. Typical network and internetwork crossings of the slit are marked (network: dotted; internetwork: dashed) as well as a brightening event in the internetwork near spatial position 170″. The radiance scale refers to the bottom curve. (An active region south of the slit – on the right – may have led to the general trend of the spectral radiance; see text.) Later measurements obtained with a cadence of 43 s are displaced successively by a factor of 1.5 for display purposes. An approximate time scale is given on the right. It should be mentioned – without further discussion – that some of the brightenings (near positions 40″ and 280″) exhibit an apparent velocity along the slit. (The solar rotation compensation of the instrument was not activated, but the slit moved only by about 3″ with respect to the network during the run.) **b)** Near-simultaneous observations at 81.15 nm. The format of the presentation is the same, but the data are smoothed over four pixels.

wavelength. The mean brightness temperatures shown here are in nearly perfect agreement with OSO-6 and Skylab results calculated from the observed disk-centre radiances (VAL81). It has been known since 1959 that the network has higher temperatures than the internetwork (de Jager 1959; Osterbrock 1961; Simon & Leighton 1964). The first spatially-resolved observation of the H I Lyman continuum near 89.6 nm across network and internetwork areas (Reeves et al. 1974) showed a peak-to-valley ratio just above ten, which is consistent with the data in Fig. 9a for 90.0 nm. Converted to brightness temperatures, this gives a $\Delta T \approx 600$ K between maximum and minimum values at the head of the continuum, and this is what we find in Fig. 12. At 71 nm the difference is about 1000 K. Of course, the average network and internetwork temperatures have a much smaller difference (approximately 200 K). Note, however, that these average values are not too well defined as they critically depend on the selection of the network and internetwork areas. In all cases, the temperatures are increasing with decreasing wavelengths.

Between 75 nm and 91 nm the slopes are also relatively constant. Except for the minimum temperature, there appears to be an increase in the slope at shorter wavelengths. This increase can directly be attributed to the steep kinetic electron

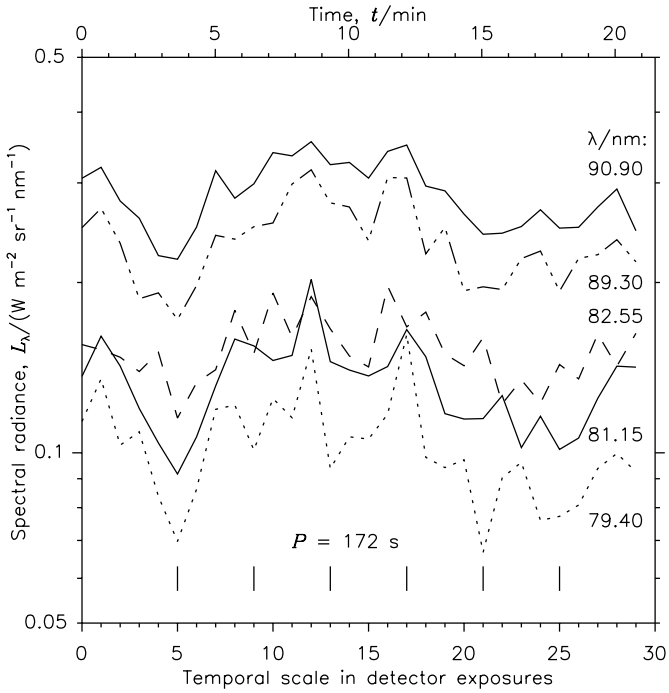

Fig. 10. Temporal variations of the maximum spectral radiances of brightenings near spatial position $s = 170''$ in Fig. 9 (marked by plus signs). Five narrow wavelength bands of the H I Lyman continuum are displayed with bandpasses of ≈0.22 nm each.

temperature increase in the upper chromosphere that has been noted shortwards of 75 nm in Sect. 3.2 and Fig. 2. More interesting is however the tentative result that both the kinetic temperatures and the departure coefficients of the network and internetwork regions reverse their orders in this range. If the spectral radiances of the fits in Fig. 2 are converted into brightness temperatures the correspondence is not perfect, especially at the shortest wavelengths. In this range the differences in the brightness temperatures are about 300 K. The maximum curve has been neglected in this assessment, because it is not relevant for the averaged spectra. Considering that the uncertainty of the measurements is about 100 K, it is probably justified to interpret the differences between late 1996 and mid 1999 as a solar effect (for instance, a variation with magnetic activity). Radiance increases of the H I Lyman continuum and of emission lines in quiet-Sun areas during the rising phase of the sunspot cycle between 1996 and 1999 have been reported by Schühle et al. (2000).

Recent simulations of Carlsson & Stein (2002), which include a coronal upper boundary condition with helium radiation and a prescribed boundary temperature, indicate that the upper chromosphere may be heated by radiation in the helium continua. The empirical model of Avrett et al. (1994) also suggests heating of the upper chromosphere by helium radiation. Since this radiation is dependent on the solar cycle (cf., McMullin et al. 2002; Floyd et al. 2002) it could be a cause of the change in slope between 1996 and 1999.

It should be pointed out that there is also a slight discrepancy at the long-wavelength side of the Lyman continuum. Compared to the spectra of 1996, the November 2001 data appear to be too low by about 150 K. The network spectral radiance near 91 nm in Fig. 2 shows an increase by a factor of 1.3 (corresponding to $\Delta T \approx 80$ K) with respect to that obtained from a quiet-Sun reference spectrum in November 2001. The deviation of ≈70 K could be related to the trend in Fig. 9 that is thought to be caused by a nearby active region. If only the northern half of the slit were taken into account, the average network temperature would increase by ≈80 K.

There is a tendency for larger differences of the brightness temperatures between network and internetwork regions at shorter wavelengths ($\Delta T = 175$ K at 90.9 nm and 300 K at 70.9 nm). The same is true for the excursions related to brightening events, which increase from $\Delta T = 120$ K at 90.9 nm to 175 K at 79.4 nm (calculated from $R_{\max}$ of Table 2). However, the latter effect is statistically only marginally significant, considering the uncertainty in the evaluation of the precision in Table 2. The important statement is that even the most pronounced brightenings observed in internetwork regions are not accompanied by brightness temperature changes of more than 200 K in the Lyman continuum ($\lambda \geq 76$ nm). These variations are comparable to the difference between mean network and internetwork temperatures.

The quasi-oscillatory episodes depicted in Fig. 5 also have peak-to-peak variations of the brightness temperature of less than 200 K. It has already been pointed out that only very few such oscillations could be detected. As the oscillations are present in internetwork regions in most SUMER observations of continua and emission lines with lower formation temperatures (Carlsson et al. 1997; Hansteen 1997; Wikstøl et al. 2000; Judge et al. 2001; but see McIntosh et al. 2001 for counter-examples), it must be concluded that their propagation or dissipation is severely affected somewhere below the Lyman-continuum emission height. It is tempting to assume that this happens at the "magic height" described by Fleck & Deubner (1989). Considering the similarity of the Lyman-continuum image in Fig. 1 with the O III structures and the difference between the silicon and hydrogen continua, magnetic fields of a canopy type in the upper chromosphere may offer a solution, as has been speculated by Carlsson et al. (1997). Mode conversion from acoustic to faster hydromagnetic waves near the transition from high to low β regimes ($\beta = 8\pi p_{\rm g}/B^2$; where $p_{\rm g}$ is the gas pressure and B the magnetic field strength) (McIntosh et al. 2001) could then explain the missing phase lag in Fig. 8. One could go so far as to question the canonical definition of the chromosphere/transition-region interface based on the steep temperature rise above 25 000 K, and ask whether a morphological criterion should be applied based on the magnetic structure.

Another explanation could be geometrical damping of the acoustic waves. These waves were modelled as plane waves by Carlsson & Stein (1995, 2002) but are shown by observations of grains at 160 nm, the H_{2v} and K_{2v} emission peaks and the C, N and O emission lines observed with SUMER (Carlsson et al. 1997) to propagate as spherical waves emanating from small source regions in the photosphere (Kalkofen 2002).

A magnetic-field topology would offer an understanding of the large spatial coherence of certain velocity oscillations discussed in Sect. 1. Although Krijger et al. (2001) have argued

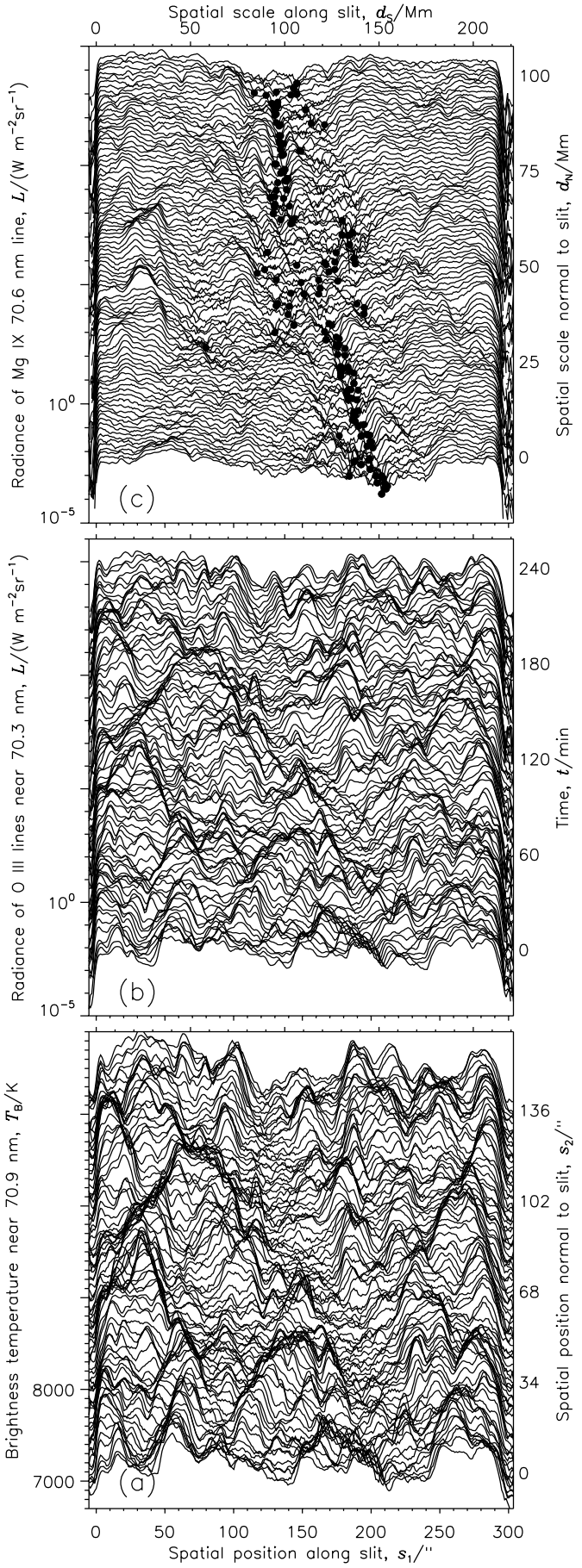

Fig. 11. Simultaneous observations of the upper chromosphere, the transition region and the corona (Sequence 5) on 10 June 1999 starting at 12:11 UTC (t = 0 min). **a)** Variations of the H I Lyman continuum near 70.9 nm along the 1″ × 300″ slit are plotted as brightness temperature for 97 step positions of a raster scan (step width: 1.14″; north is towards left and west is up). The temperature scale refers to the bottom curve. Subsequent slit positions are shifted upwards (by 45 K each) resulting in a spatial scale for the second dimension on the right-hand side. Note that detector pixels not illuminated by the slit image (s_1 < 0″ or s_1 > 300″) provide information on the background levels. They correspond to 6700 K, slightly below the coronal hole values. **b)** The network structure seen in the O III multiplet near 70.3 nm is shown in a format similar to the bottom panel. The logarithmic radiance scale applies to the bottom curve. Subsequent slit positions are shifted upwards by a factor of 1.5. The axis on the right-hand side represents the temporal scale during the scan of the instrument. Here the background level is more than an order of magnitude below the weakest signal. **c)** The coronal structure above the network region is displayed in the upper panel. Again the format is similar to the other ones, but the spatial scale normal to the slit is in units of megametre. This scale combines the pointing changes and the solar rotation during the scan. Black dots in the central area of this diagram indicate regions with a very low radiance in the Mg IX line, yet well above the detector background. These dots outline the position of the coronal hole. Near the middle of the display, it can be seen that one step position is missing. The reason is a telemetry error at 14:34 UTC, which had to be eliminated.

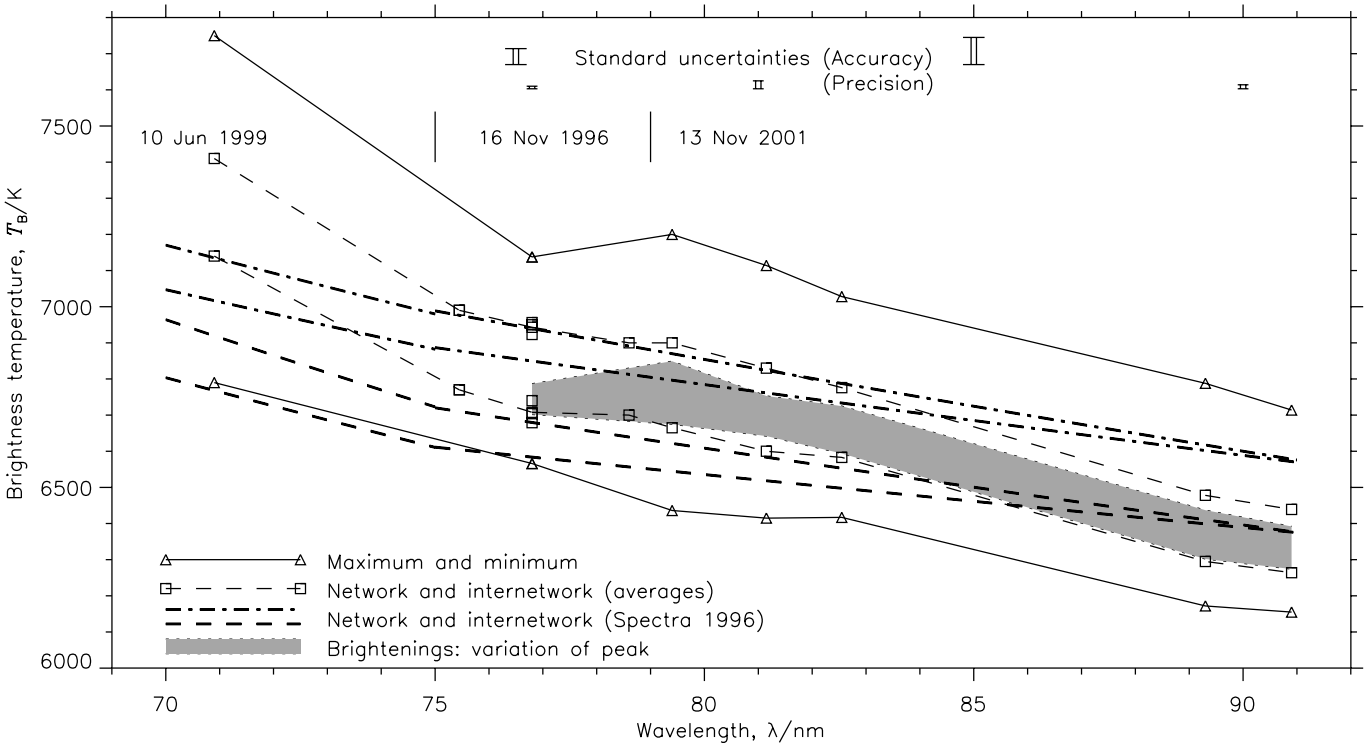

Fig. 12. Brightness temperatures of the H I Lyman continuum in the upper chromosphere as a function of wavelength. The maximum and minimum values are plotted by solid lines with actual data points shown by triangles. The average network and internetwork brightness temperatures are given as thin dashed lines indicating that network values are 200 K to 300 K higher than the internetwork ones. Brightening events could be observed in the wavelength range from 77 nm to 91 nm in this study with temperature variations of typically 150 K (shaded area). The precision of the observations made on a certain date is rather high (the standard uncertainties are determined from the counting statistics of the mean values), whereas measurements obtained in different years are subject to the larger uncertainties related to their accuracy. The range of brightness temperatures in 1996 (Sequence 1) resulting from the slopes of the H I Lyman continuum in Fig. 2 are added as thick dashed lines (internetwork) and thick dashed-dotted lines (network). Note their excellent agreement with the November 1996 data near 77 nm (Sequence 3).

that the increased coherence length might be a consequence of a very compressed time slice of the presentations, the effect appears to be real, because at least in Fig. 5 of Hansteen et al. (2000), the time scale is not compressed, and yet the velocity oscillations in C III are spatially coherent over the entire internetwork section of 20″ to 30″.

These findings are consistent with results discussed above suggesting that – in contrast to portions of the lower chromosphere – the upper chromosphere is not heated by the waves and oscillations seen in the chromosphere, which are presumably of acoustic nature (Jordan 1977; Athay & White 1978). Instead, in accord with the observations by Steffens et al. (1996) that grains supply only 9% of the K_{2v} emission of the internetwork chromosphere, they indicate that dissipation contributed by acoustic oscillations is not the main heating mechanism of the internetwork upper chromosphere. Osterbrock (1961) proposed hydromagnetic waves to be important at greater heights.

Vernazza et al. (1975) and Bruner (1978) occasionally found acoustic waves even in the transition region, but concluded on the basis of the low wave intensity that they are not important for heating the corona. With reference to Figs. 7 and 8 it can, in addition, be said that even strong transition-region events in general do not show a signature in the overlying coronal layers. This is in line with the low correlation coefficients found for the coupling between the transition region and the corona. Such a decoupling of the corona from the transition region has also been deduced from spectroscopic observations (Feldman 1983), and appears to be a consequence of the magnetic-field topology.

Acknowledgements. The SUMER instrument and its operation are financed by the Deutsches Zentrum für Luft- und Raumfahrt (DLR), the Centre National d'Etudes Spatiales (CNES), the National Aeronautics and Space Administration (NASA), and the European Space Agency's (ESA) PRODEX programme (Swiss contribution). The instrument is part of SOHO, ESA's and NASA's Solar and Heliospheric Observatory. This work was supported by the Smithsonian Institution, NASA, the National Science Foundation, and the Max-Planck-Gesellschaft. We thank Ingolf E. Dammasch for help with the image processing task.

References

Athay, R. G., & White, O. R. 1978, ApJ, 226, 1135
Athay, R. G., & Dere, K. P. 1990, ApJ, 358, 710
Avrett, E. H., Fontenla, J. M., & Loeser, R. 1994, IAU Symp., 154, 35
Ayres, T. R. 1981, ApJ, 244, 1064

Ayres, T. R. 2002, ApJ, 575, 1104
Ayres, T. R., & Rabin, D. 1996, ApJ, 460, 1042
Balmforth, N. J., & Gough, D. O. 1990, ApJ, 362, 256
Biermann, L. 1948, Z. Astrophys., 25, 161
Brekke, P., & Kjeldseth-Moe, O. 1994a, ApJ, 431, L55
Brekke, P., & Kjeldseth-Moe, O. 1994b, Sol. Phys., 150, 19
Bruner, Jr., E. C. 1978, ApJ, 226, 1140
Cally, P. S. 2001, ApJ, 548, 473
Carlsson, M., & Stein, R. F. 1994, in Chromospheric Dynamics, ed. M. Carlsson (Oslo), 47
Carlsson, M., & Stein, R. F. 1995, ApJ, 440, L29
Carlsson, M., & Stein, R. F. 1997, ApJ, 481, 500
Carlsson, M., & Stein, R. F. 2002, ApJ, 572, 626
Carlsson, M., Rutten, R. J., & Shchukina, N. G. 1992, A&A, 253, 567
Carlsson, M., Judge, P. G., & Wilhelm, K. 1997, ApJ, 486, L63
Chang, E. S., Avrett, E. H., Manas, P. J., et al. 1991, ApJ, 379, L79
Chapman, R. D., Jordan, S. D., Neupert, W. M., et al. 1972, ApJ, 174, L97
Chipman, E. G., Bruner, Jr., E. C., Shine, R. A., et al. 1976, ApJ, 210, L103
Cook, J. W., Brueckner, G. E., & Bartoe, J.-D. F. 1983, ApJ, 270, L89
Cram, L. E. 1978, A&A, 70, 345
Cram, L. E., & Damé, L. 1983, ApJ, 272, 355
Curdt, W., & Heinzel, P. 1998, ApJ, 503, L95
Curdt, W., Heinzel, P., Schmidt, W., et al. 1999, in 9th European Meeting on Solar Physics of EPS and EAS: Magnetic Fields and Solar Processes, ed. A. Wilson, ESA SP-448, 177
Curdt, W., Brekke, P., Feldman, U., et al. 2001, A&A, 375, 591
Damé, L. 1984, in Small-scale Dynamical Processes in Quiet Stellar Atmospheres, ed. S. L. Keil (Sunspot: NSO/SPO), 54
Deming, D., Jennings, D. E., McCabe, G., et al. 1992, ApJ, 396, L53
De Pontieu, B. 2002, ApJ, 569, 474
Deslandres, H. 1899, Comptes Rendus, 129, 1225
Deubner, F.-L. 1975, A&A, 44, 371
Domínguez Cerdeña, I., Kneer, F., & Sánchez Almeida, J. 2003, ApJ, 582, L55
Dowdy, Jr., J. F., Rabin, D., & Moore, R. L. 1986, Sol. Phys., 105, 35
Doyle, J. G., van den Oord, G. H. J., O'Shea, E., & Banerjee, D. 1999, A&A, 347, 335
Feldman, U. 1983, ApJ, 275, 367
Feldman, U., Dammasch, I. E., & Wilhelm, K. 2001, ApJ, 558, 423
Fleck, B., & Deubner, F.-L. 1989, A&A, 224, 245
Floyd, L., McMullin, D., & Herring, L. 2002, in Proc. SOHO 11 Symp.: From Solar Min to Max: Half a Solar Cycle with SOHO, ed. A. Wilson, ESA SP-508, 197
Foing, B., & Bonnet, R. M. 1984, ApJ, 279, 848
Gabriel, A. H. 1976, Phil. Trans. R. Soc. Lond. A, 281, 339
Goldberg, L. 1939, ApJ, 89, 673
Gouttebroze, P., Vial, J.-C., Bocchialini, K., & Leibacher, J. W. 1999, Sol. Phys., 184, 253
Hale, G. E., & Ellerman, F. 1904, ApJ, 19, 41
Hansteen, V. H. 1997, in Proc. 5th SOHO Workshop: The Corona and Solar Wind Near Minimum Activity, ed. A. Wilson, ESA SP-404, 45
Hansteen, V. H., Betta, R., & Carlsson, M. 2000, A&A, 360, 742
Harrison, R. A., Sawyer, E. C., Carter, M. K., et al. 1995, Sol. Phys., 162, 233
Heinzel, P., & Curdt, W. 1999, ASP Conf. Ser., 184, 201
Hoang-Binh, D. 1991, A&A, 241, L13
Hoekzema, N. M., Rutten, R. J., & Cook, J. W. 1997, ApJ, 474, 518
Hoekzema, N. M., Rimmele, T. R., & Rutten, R. J. 2002, A&A, 390, 681
Hofmann, J., Steffens, S., & Deubner, F.-L. 1996, A&A, 308, 192
de Jager, C. 1959, in Hdb. d. Phys., 52, ed. S. Flügge (Berlin, Göttingen, Heidelberg: Springer-Verlag), 80
Jordan, S. J. 1977, Sol. Phys., 51, 51
Judge, P. G., Carlsson, M., & Wilhelm, K. 1997, ApJ, 490, L195
Judge, P. G., Tarbell, T. D., & Wilhelm, K. 2001, ApJ, 554, 424
Kalkofen, W. 2001, ApJ, 557, 376
Kalkofen, W. 2002, ASP Conf. Ser., 286, 385
Kalkofen, W., Ulmschneider, P., & Avrett, E. H. 1999, ApJ, 521, L141
Kalkofen, W., Hasan, S. S., & Ulmschneider, P. 2003, in Dynamic Sun, ed. B. N. Dwivedi (Cambridge: Cambridge University Press), 165
Krijger, J. M., Rutten, R. J., Lites, B. W., et al. 2001, A&A, 379, 1052
Kumar, P. 1993, ASP Conf. Ser., 42, 15
Lamb, H. 1908, Proc. Roy. Soc. Lond., 7, 122
Leighton, R. B., Noyes, R. W., & Simon, G. W. 1962, ApJ, 135, 474
Lemaire, P., & Skumanich, A. 1973, A&A, 22, 61
Lemke, M., & Holweger, H. 1987, A&A, 173, 375
Lites, B. W., Rutten, R. J., & Kalkofen, W. 1993, ApJ, 414, 345
Lites, B. W., Rutten, R. J., & Berger, T. E. 1999, ApJ, 517, 1013
Liu, S.-Y. 1974, ApJ, 189, 359
Livingston, W., & Harvey, J. 1971, IAU Symp., 43, 51
McIntosh, S. W., Bogdan, T. J., Cally, P. S., et al. 2001, ApJ, 548, L237
McMullin, D. R., Judge, D. L., Hilchenbach, M., et al. 2002, in The Radiometric Calibration of SOHO, ISSI Scientific Report, SR-002, ed. A. Pauluhn, M. C. E. Huber, & R. von Steiger (Noordwijk: ESA Publications Division), 135
Menzel, D. H. 1937, ApJ, 85, 330
Muglach, K., Fleck, B., Schühle, U. 2000, Adv. Space Res., 25, 1731
Noyes, R. W. 1967, IAU Symp., 28, 293
Noyes, R. W., & Leighton, R. B. 1963, ApJ, 138, 631
Noyes, R. W., & Kalkofen, W. 1970, Sol. Phys., 15, 120
Orrall, F. Q. 1966, ApJ, 143, 917
Osterbrock, D. E. 1961, ApJ, 134, 347
Parker, E. N. 1963, ApJ, 138, 552
Patsourakos, S., Vial, J.-C., Gabriel, A. H., & Bellamine, N. 1999, ApJ, 522, 540
Patsourakos, S., & Vial, J.-C. 2002, A&A, 385, 1073
Pottasch, S. R. 1963, ApJ, 137, 945
Pottasch, S. R., & Thomas, R. N. 1959, ApJ, 130, 941
Reeves, E. M. 1976, Sol. Phys., 46, 53
Reeves, E. M., Foukal, P. V., Huber, M. C. E., et al. 1974, ApJ, 188, L27
Rosenthal, C. S., Bogdan, T. J., Carlsson, M., et al. 2002, ApJ, 564, 508
Rutten, R. J., & Uitenbroek, H. 1991, Sol. Phys., 134, 15
Schatzman, E., & Souffrin, P. 1967, ARA&A, 5, 67
Schühle, U., Brekke, P., Curdt, W., et al. 1998, Appl. Opt., 37, 2646
Schühle, U., Wilhelm, K., Hollandt, J., et al. 2000, A&A, 354, L71
Smith, P. L., & Huber, M. C. E. 2002, in The Radiometric Calibration of SOHO, ISSI Scientific Report, SR-002, ed. A. Pauluhn, M. C. E. Huber, & R. von Steiger (Noordwijk: ESA Publications Division), 21
Schwarzschild, M. 1948, ApJ, 107, 1
Simon, G. W., & Leighton, R. B. 1964, ApJ, 140, 1120
Sivaraman, K. R., & Livingston, W. C. 1982, Sol. Phys., 80, 227
Solanki, S. K. 1993, Space Sci. Rev., 63, 1
Solanki, S. K., Livingston, W., & Ayres, T. 1994, Science, 263, 64
Solanki, S. K., Livingston, W., Muglach, K., & Wallace, L. 1996, A&A, 315, 303
Steffens, S., Hofmann, J., & Deubner, F. L. 1996, A&A, 307, 288
Steffens, S., Deubner, F.-L., Fleck, B., et al. 1997a, in Proc. 5th SOHO Workshop: The Corona and Solar Wind Near Minimum Activity, ed. A. Wilson, ESA SP-404, 679

Steffens, S., Deubner, F.-L., Fleck, B., & Wilhelm, K. 1997b, in Proc. 5th SOHO Workshop: The Corona and Solar Wind Near Minimum Activity, ed. A. Wilson, ESA SP-404, 685
Stenflo, J. O. 1973, Sol. Phys., 32, 41
Stuart, F. E., & Rush, J. H. 1954, ApJ, 120, 245
von Uexküll, M., & Kneer, F. 1995, A&A, 294, 252
Uitenbroek, H. 2000, ApJ, 531, 571
Uitenbroek, H., Noyes, R. W., & Rabin, D. 1994, ApJ, 432, L67
Ulmschneider, P., & Kalkofen, W. 2003, in Dynamic Sun, ed. B. N. Dwivedi (Cambridge: Cambridge University Press), 181
Ulrich, R. K. 1970, ApJ, 162, 993
Vernazza, J. E., Foukal, P. V., Huber, M. C. E., et al. 1975, ApJ, 199, L123
Vernazza, J. E., Avrett, E. H., & Loeser, R. 1981, ApJS, 45, 635 (VAL81)
Warren, H. P., Mariska, J. T., & Wilhelm, K. 1998, ApJS, 119, 105
Wikstøl, Ø., Hansteen, V. H., Carlsson, M., & Judge, P. G. 2000, A&A, 531, 1150
Wilhelm, K. 2002, in The Radiometric Calibration of SOHO, ISSI Scientific Report, SR-002, ed. A. Pauluhn, M. C. E. Huber, & R. von Steiger (Noordwijk: ESA Publications Division), 37
Wilhelm, K., Curdt, W., Marsch, E., et al. 1995, Sol. Phys., 162, 189
Wilhelm, K., Lemaire, P., Dammasch, I. E., et al. 1998, A&A, 334, 685
Wilhelm, K., Schühle, U., Curdt, W., et al. 2002, in The Radiometric Calibration of SOHO, ISSI Scientific Report, SR-002, ed. A. Pauluhn, M. C. E. Huber, & R. von Steiger (Noordwijk: ESA Publications Division), 145
Worden, J., Harvey, J., & Shine, R. 1999, ApJ, 523, 450
Zirin, H., & Popp, B. 1989, ApJ, 340, 571